Paper No. 176

ISMS 2016

Influence of weak planes on rockburst occurrence

Amin Manouchehrian, Ming Cai *

Bharti School of Engineering, Laurentian University, Sudbury, Canada, P3E 2C6
MIRARCO, Laurentian University, 935 Ramsey Lake Road, Sudbury, Canada P3E 2C6
State Key Laboratory of Geomechanics and Geotechnical Engineering, Institute of Rock and Soil Mechanics, Chinese Academy of Sciences, Wuhan, 430071, China

ABSTRACT
Geological structures such as faults, joints, and dykes have been observed near excavation boundaries in many rockburst case histories. In this paper, the role of weak planes around tunnels in rockburst occurrence was studied. The Abaqus-Explicit code was used to simulate dynamic rock failure in deep tunnels. Firstly, the tool's usefulness for modelling geomaterials was improved by introducing material heterogeneity using Python scripting. The modelling results showed that heterogeneous models resulted in more realistic failure modes than homogeneous models. Secondly, rock failure near the excavation boundary of a tunnel without any adjacent geological structure was modelled and released kinetic energy from rock due to failure and velocity of failed elements at the tunnel wall were calculated. Then, a weak plane was added to the model. This resulted in more released kinetic energy and higher element velocity, indicating that rock failure became more violent in the models with weak planes. The modelling results confirm that the presence of geological structures in the vicinity of deep excavations is a necessary condition for the occurrence of rockburst. It can be used to explain localized rockburst occurrence in civil tunnels and mining drifts. The methodology for rockburst analysis presented in this paper can be useful for rockburst anticipation and control during mining and tunneling in highly stressed grounds.
KEYWORDS: Numerical simulation; excavation; heterogeneity; weak plane; rockburst

1. INTRODUCTION

Rockburst is an unstable and violent rock failure, and one of the most hazardous problems in deep mines and civil tunnels. Rockburst is associated with rapid ejection of broken rocks and is accompanied by a large amount of energy release (Hedley et al., 1992; Andrieux et al., 2013). The rockburst problem increases as mining activities progress to deeper grounds. Some efforts have been made to understand why rockburst happens, to anticipate where it will happen, and to predict how large a rockburst event will be. Having this knowledge would be valuable for rock support design.

Rockburst case histories reveal that rockburst damage locations are not uniform. In the other words, damage extent in a tunnel caused by a rockburst varies at different locations. The localized rockburst phenomenon originates from the complex mechanism that drives rockburst and the contribution of different factors on rockburst occurrence. Many factors that influence rockburst damage have been identified (Kaiser and Cai, 2012) but no one knows the exact conditions for the occurrence of a rockburst in a complex underground setting. Studies have documented the presence of geological structures such as faults, shears, and dykes in vicinity of rockburst locations (Hedley et al., 1992); however, their role in rockburst occurrence and damage is not well understood.

Numerical models have been used to simulate unstable rock failure in laboratory tests (Kias and Ozbay 2013; Manouchehrian and Cai, 2016) and underground openings (Jiang et al., 2010; Gu and Ozbay 2015). A missing factor in the previous numerical works is the influence of geological structures on rockburst occurrence and damage. In this paper, the influence of weak planes (e.g. faults and shears) on rockburst occurrence and damage around underground openings is investigated using Finite Element Method (FEM).

2. ROCK FAILURE SIMULATION USING ABAQUS

Unstable rock failure is a dynamic phenomenon and should be treated as a nonlinear dynamic problem. Studies have shown that the explicit numerical method is more suitable than the implicit numerical method for solving nonlinear dynamic problems because the problem of convergence is eliminated. Abaqus is a FEM-based numerical tool which is equipped with implicit and explicit solvers, making it applicable for solving a large variety of physical and engineering problems (Dassault System, 2010). Manouchehrian and Cai (2016) simulated

*Corresponding author – email : mcai@laurentian.ca

uniaxial and poly-axial compression tests using the Abaqus-Explicit tool and demonstrated the suitability of the tool for simulating unstable or dynamic rock failure. In this study, this tool is used to simulate rockburst in deep tunnels.

Despite Abaqus's capability for simulating a large variety of engineering problems, its application in the geomechanical field is limited. A key characteristic of geomaterials is material heterogeneity, which cannot be readily modelled in Abaqus through GUI. Fortunately, Abaqus provides windows for adding and improving its capability using scripting and programming. Hence, for modelling rock-like materials, it is possible to introduce material heterogeneity into the models to produce more realistic results. In this section, a simulation of rock failure processes in compression using homogeneous material models is presented first, followed by an introduction of material heterogeneity into Abaqus models and a simulation of rock failure processes in compression using heterogeneous material models.

2.1 Homogeneous model

To study the failure mechanism using Abaqus, the laboratory tested mechanical properties of T_{2b} marble (Table 1) are used as the base case. T_{2b} marble is the host rock of the diversion tunnels at the Jinping II hydropower station in China (Zhang et al., 2012).

Unconfined and confined compression tests are simulated to investigate the failure mechanism of homogeneous rocks. An elasto-plastic Mohr-Coulomb strain-softening model with homogeneous material properties is used to model the strength behaviour of the T_{2b} marble. Table 2 presents the calibrated parameters for defining the strain-softening behaviour of the rock in the homogeneous model. A rectangular specimen with a height of 250 mm and a width of 100 mm is used for the simulation. In the unconfined compression test simulation, one end of the specimen is fixed in the maximum stress direction and the other direction is free (roller constraint) and a constant velocity of 0.03 $m.s^{-1}$ is applied directly to the other end to load the specimen. The same end boundary conditions are applied to the specimens in the confined compression test simulation and the confinements applied are 5, 10, 20, and 40 MPa. In the developed homogeneous model, a uniaxial compressive strength (UCS) of 113.6 MPa, a friction angle of 30°, and a cohesion of 32.9 MPa are calculated, which are similar to the reported laboratory test data (Table 1).

Figure 1b shows the failure pattern in the homogeneous models indicated by the maximum principal plastic strain. The figure shows that confinement does not affect the failure pattern in the homogeneous model because all of them show distinct shear failure. Despite that the mechanical parameters of the T_{2b} marble are captured by the homogeneous model, it fails to capture the splitting failure under low confinement.

Table 1: Physical and mechanical properties of the T_{2b} marble (Zhang et al., 2014).

Parameter	Value
Density, ρ (kg.m^{-3})	2780
Young's modulus, E (GPa)	55
Poisson's ratio, ν	0.27
Uniaxial compressive strength, *UCS* (MPa)	110.7*
Cohesion, c (MPa)	32.6
Friction angle, φ (°)	29

* UCS of the T_{2b} marble was reported between 100 and 160 MPa in (Zhang et al., 2014). This value was calculated according to $UCS = \frac{2c.cos\varphi}{(1-sin\varphi)}$ for the present study.

Table 2: Strain-softening parameters of the homogeneous model.

Cohesion		Tension cut-off	
Cohesion yield stress (MPa)	Shear plastic strain	Tension cut-off stress (MPa)	Tensile plastic strain
32.2	0	5.5	0
0.01	0.2	0.1	0.001

2.2 Heterogeneous model

In order to introduce heterogeneity into models, the material properties of each element are assigned randomly following normal distribution functions. The introduction of material heterogeneity cannot be conducted using the GUI and Python scripting is needed.

The developed Python script assigns randomly distributed material properties of E, c, and φ to the elements and the properties follow normal distribution functions. One example of execution of the developed technique to simulate a rectangular model with 4000 elements and 100 materials is presented in Figure 2 (each color represents one material). In this figure, μ and σ are the averages and the standard deviations of each parameter (E, c, and φ).

Heterogeneous model is used to simulate the mechanical properties of the T_{2b} marble (Table 1). A UCS of 113.5 MPa, a friction angle of 29.7° and a cohesion of 32.7 MPa are estimated for the heterogeneous model, which are similar to the laboratory test results.

Figure 1a shows photographs of the failed T_{2b} marble specimens in laboratory tests (Zhang et al., 2014) and Figure 1c presents snapshots of the plastic strain obtained by the numerical models. It is seen that in the heterogeneous model, the failure modes change from splitting failure at zero confinement to shear failure at high confinements. The homogeneous material models cannot capture axial splitting at zero confinement but the heterogeneous material model successfully captures this failure mode. Hence, the developed heterogeneous material model in Abaqus enhances its capability for adding value to the tool in solving geotechnical engineering problems.

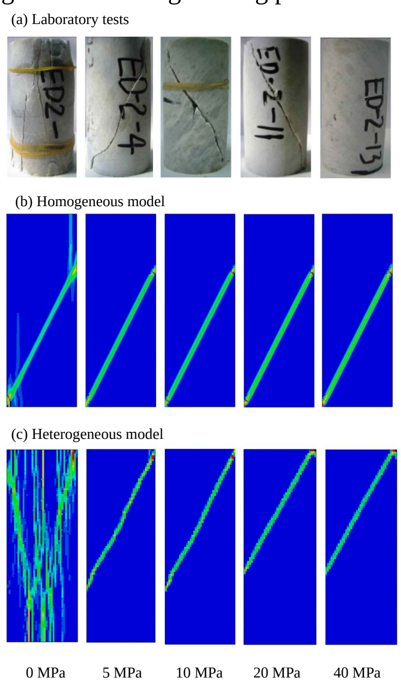

Figure 1: Failure patterns at different confinements from (a) laboratory tests (Zhang et al., 2014), (b) homogeneous model, and (c) heterogeneous model.

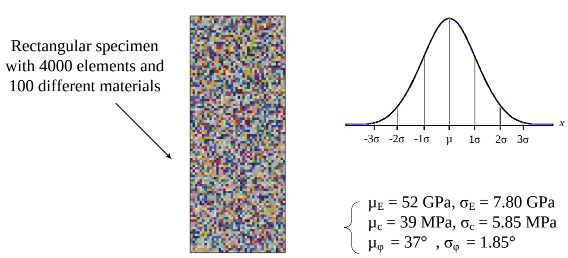

Figure 2: Generated heterogeneous material in Abaqus by Python scripting.

3. ROCKBURST SIMULATION

In this section, models are developed to study the influence of weak planes on rockburst occurrence and damage numerically. A circular tunnel with a radius (*r*) of 5 m is modelled. In the numerical models, the outer boundary width and height should be at least ten times of the tunnel diameter to exclude the effect of the outer boundary on stress redistribution around the tunnel. In this study, the models also include a fault with a varying length. Hence, the outer boundary width and height are 15 times of the tunnel diameter to ensure that stress redistribution around the fault does not affect the modelling results. Figure 3 illustrates the model geometry.

Before any excavations, in situ stresses are applied to the outer boundaries and then the boundaries are fixed with roller constraints. Tunnel excavation is then simulated. The horizontal (σ_x) and vertical (σ_z) in situ stresses are assumed to be 30 and 60 MPa, respectively. Gradual excavation of the tunnel is simulated by stress reduction at the tunnel boundary in ten steps.

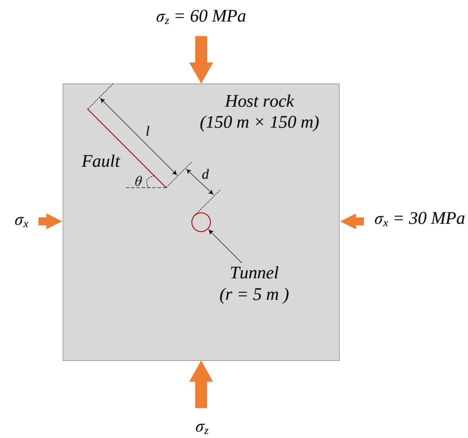

Figure 3: Model geometry and boundary conditions.

An elasto-plastic Mohr-Coulomb strain-softening model with heterogeneous material properties is used to model a rock mass with its physical and mechanical properties presented in Table 3. In the developed heterogeneous model, the mean values of *E*, *c*, and φ are 21 GPa, 22 MPa, and 31°, respectively and coefficients of variation (COV) of them are 5%. The adjusted parameters for defining the strain-softening behaviour of the rock mass are presented in Table 4.

Table 3: Physical and mechanical properties of the rock mass.

Parameter	Value
Density, ρ (kg.m^{-3})	2500
Young's modulus, *E* (GPa)	20
Poisson's ratio, ν	0.2
Uniaxial compressive strength, *UCS* (MPa)	69.3
Cohesion, *c* (MPa)	20
Friction angle, φ (°)	30

Table 4: Parameters with COV = 5% for defining the post-peak behaviour of the rock mass.

Cohesion		Tension cut-off	
Cohesion yield stress (MPa)	Shear plastic strain	Tension cut-off stress (MPa)	Tensile plastic strain
22.0	0	3.0	0
0.01	0.2	0.1	0.005

Firstly, a tunnel without any adjacent geological structure is modelled. Shear and tensile failures around the tunnel, indicated by the maximum principal plastic strains, are illustrated in Figure 4. The figure shows a symmetric failure around the tunnel, with shear failure zones located at 3 and 9 o'clock because the maximum in situ principal stress direction is vertical.

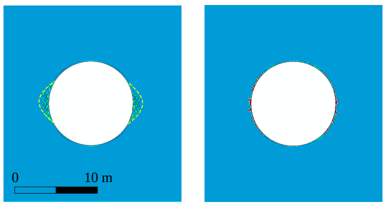

(a) Shear failure (b) Tensile failure

Figure 4. Failure zones around the tunnel without any nearby geological structures.

Figure 5a shows the velocity of elements around the tunnel at the beginning of Step 10 (at the time of failure). The figure shows a maximum velocity of 1.78 $m.s^{-1}$ in one node at the tunnel surface. The minimum velocity of the failed elements is 0.14 $m.s^{-1}$. In this study, the velocity of all failed elements around the tunnel during the running time is tracked and then an average velocity (V_{max}) is calculated. The maximum of the average velocity ($\overline{V}_{max}$) during the running time is picked to interpret the results. In this case, the average of maximum velocity of the failed elements around the tunnel ($\overline{V}_{max}$) is 0.58 $m.s^{-1}$. When failure is stable, the ejection velocity of the failed rocks is low (Milev et al., 2002). The maximum kinetic energy per unit volume (KE_{max}) from the failed rocks, which can be used as an indicator of rock failure intensity, is 0.65 $kJ.m^{-3}$. In this case, failure can be considered as stable; if it were in the field, the failure would be in the form of spalling, spitting, or shallow slabbing.

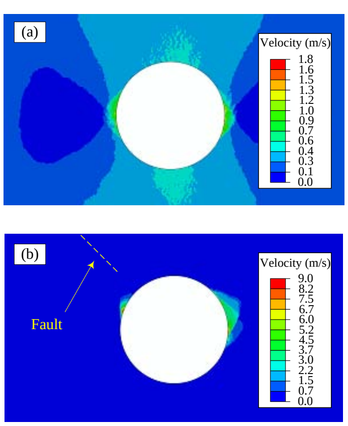

Figure 5: Velocity of the elements in the models (a) without and (b) with a nearby fault.

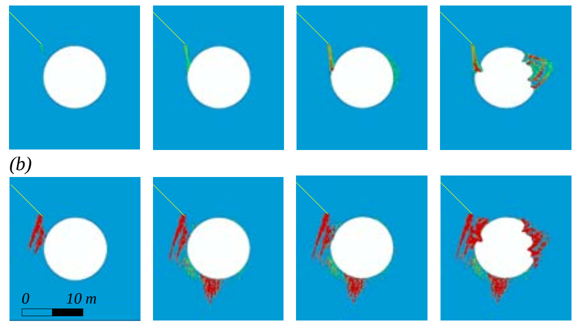

Figure 6: Failure development around the tunnel with a nearby fault: (a) shear failure, (b) tensile failure (l = 80 m, d = 2.5 m, and θ = 45°).

Next, a fault with a dip of θ = 45°, a length of l = 80 m and at a position of d = 2.5 m from the tunnel wall is added to the model (see Figure 3). A Coulomb model with a friction coefficient of 0.4 and zero cohesion is used to model the fault.

Development of failure around the tunnel at Steps 1, 4, 9, and 10 is shown in Figure 6. The figure shows initiation of tensile and shear fractures at the tip of the fault at Step 1 excavation. Then, the shear fractures propagate toward the tunnel face (Step 4) and rocks between the fault and the tunnel are ruptured. Meanwhile, tensile fractures are initiated at the bottom of the tunnel. Figure 7 shows the relative movement of the fault at four different points along the fault (the fault tip and three other points at a distance of 1 m from each other). A relative slip of the fault of about 25 mm occurs at point p-1 after the excavation is completed. The slip rate is the highest at Step 9. Slip of the fault due to excavation causes compression at positions of 1 to 4 o'clock (Step 9).

At Step 10, the failed rocks on the right tunnel wall would blow out violently with a $\overline{V}_{max}$ = 3.4 $m.s^{-1}$ (Figure 5b) and a failure pit with a depth of 3 m would be created. The maximum unit kinetic energy

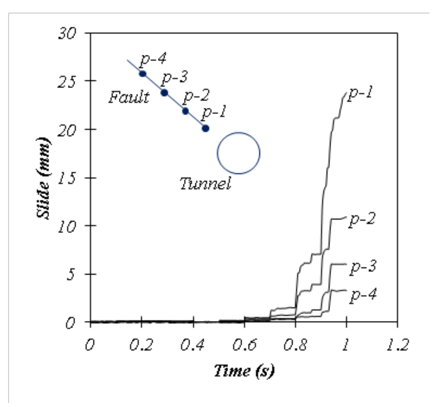

Figure 7: Relative movement of the fault during the running time.

is 6.97 kJ.m^{-3}.

Tunneling near a fault with different fault lengths is simulated to understand the influence of the fault length (l) on rockburst damage. The length of the fault (l) is varied at l = 0, 20, 40, 60, and 80 m, resulting in l/r ratios of 0, 4, 8, 12, and 16, respectively. The same modelling procedure described above is used.

The influence of l on $\overline{V}_{max}$ and KE_{max} is presented in Figure 8. The figure indicates that an increase in the fault length results in increases of both $\overline{V}_{max}$ and KE_{max}. According to Figure 8, when l = 0 (i.e. there is no fault), the V_{max} is low (0.58 m.s^{-1}) and the rock failure can be considered as stable. $\overline{V}_{max}$ and KE_{max} increase rapidly as the l/r ratio increases. For example, for l/r = 16, $\overline{V}_{max}$ = 3.4 m.s^{-1} and KE_{max} = 6.97 kJ.m^{-3}, which indicates that the rock failure is more violent than the models with shorter fault length. In such a case it can be expected that a rockburst is likely to occur. The failure zones around the tunnel for various l/r ratios are presented in Figure 9, with tensile and shear failure zones shown separately. It is seen that as the l/r ratio increases, the failure zone becomes large.

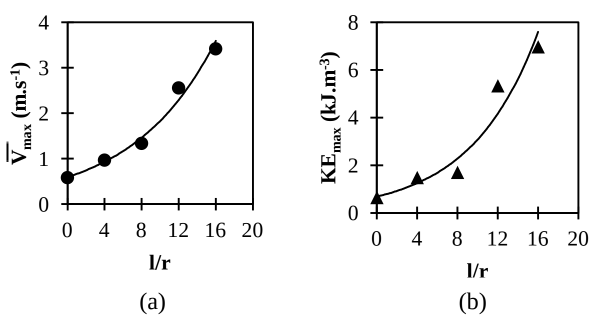

Figure 8: Influence of fault length on (a) $\overline{V}_{max}$ and (b) KE_{max}.

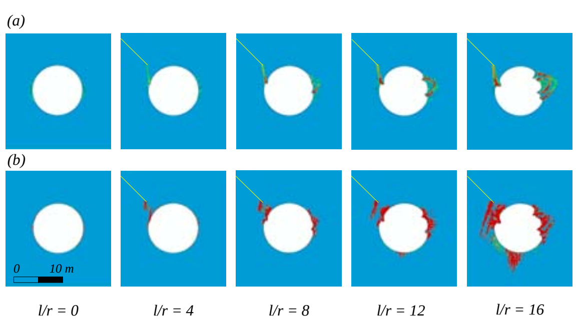

Figure 9: Failure zones around the tunnel in models with different fault lengths: (a) shear failure, (b) tensile failure.

Figure 10 shows the total displacement distribution around the tunnel at the end of Step 9 excavation (before the sidewall fails). The figure shows that when the fault is longer, a larger volume of hanging wall rock can move toward the tunnel and push the rocks near the tunnel wall boundary, particularly the rocks on the right wall side. Hence, more strain energy release is possible if there is a sudden rock failure. This explains why the unit maximum kinetic energy is high for large l/r ratios. Furthermore, the displacement field also indicates that the mine system stiffness is low when the l/r ratio is high because the rocks surrounding the failed rocks can have more deformation.

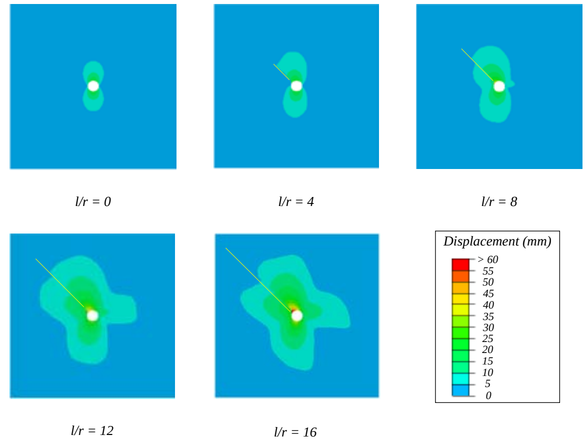

Figure 10: Displacement around the tunnel in models with different fault lengths.

The concept of mine system stiffness has been used by some researchers to explain rockburst in underground mines (Aglawe, 1999; Wiles, 2002). Although it is difficult to calculate mine system stiffness quantitatively in a tunnel setting, an analogy to Loading System Stiffness (LSS) in laboratory testing can be made. Laboratory test results show that the modes of failure (stable and unstable) depend on the relative stiffness of the rock and the loading system (Wawersik and Fairhurst, 1970). A soft loading system is capable of storing more strain energy than a stiff loading system. Thus when a rock specimen fails, the failure is stable under a stiff loading system and unstable under a soft loading system. Despite the difference in the loading in the field and in laboratory, it can be seen that an increase of l decreases the mine system stiffness and as a result, unstable rock failure can happen around the tunnel. This can be clearly seen from the results presented in Figure 8 to Figure 10.

Reduced mine system stiffness can be considered as a main effect of weak planes near openings in deep underground mines, which can potentially lead to rockburst. According to the simulation results, it is seen that the size of a weak plane is an important factor that influences rockburst damage.

4. CONCLUSION

In this paper, the Abaqus-Explicit code was used to study the role of weak planes in rockburst occurrence and damage. Firstly, Abaqus's usefulness for modelling geomaterials was improved by introducing material heterogeneity using Python scripting. The modelling results showed that heterogeneous models resulted in more realistic failure modes than homogeneous models. Secondly, rock failure near the excavation boundary of a tunnel without any adjacent geological structure was modelled and the released kinetic energy due to rock failure and velocities of elements at the tunnel boundaries were calculated. When a weak plane was added to the model, it resulted in more released kinetic energy and higher element velocity, indicating that rock failure became more violent in the model with the weak plane. The modelling results indicated that the failure became more violent when the weak plane length was longer.

It was shown that weak planes around a tunnel may change the loading system stiffness of the failed rocks and induce rockburst because when there is a weak plane near an underground opening, a large volume of rock is able to move. The approach presented in this study can capture dynamic response of a rock mass. In particular, the ability to estimate ejection velocity and released kinetic energy provides a new approach for dynamic rock support design.

5. ACKNOWLEDGEMENT

Financial supports from the Natural Sciences and Engineering Research Council (NSERC) of Canada, Vale, LKAB, CEMI, MIRARCO, and the Open Research Fund of the State Key Laboratory of Geomechanics and Geotechnical Engineering, Institute of Rock and Soil Mechanics, Chinese Academy of Sciences (Grant NO. Z015001) for this work are gratefully acknowledged.

6. REFERENCES

Aglawe, J. (1999) Unstable and Violent Failure around Underground Openings in Highly Stressed Ground. Queen's University.

Andrieux, P., Blake, W., Hedley, D. G. F., Nordlund, E., Phipps, D., Simser, B., and Swan, G. 2013. Rockburst Case Histories: 1985, 1990, 2001 & 2013, Sudbury, Ont: CAMIRO Mining Division for the Deep Mining Research Consortium; 2013.

Dassault System, (2010). ABAQUS 6.10 Users' manual. Providence, RI, USA: HKS Inc.

Gu, R., and Ozbay, U. (2015) Numerical investigation of unstable rock failure in underground mining condition. Computers and Geotechnics, Volume 63, pp. 171-182.

Hedley, D. G. F., Mineral, C. C. f., Technology, E., Association, O. M., and Laboratories, M. R. (1992) Rockburst Handbook for Ontario Hardrock Mines: Energy, Mines and Resources Canada, Canada Center for Mineral and Energy Technology.

Jiang, Q., Feng, X.T., Xiang, T. B., and Su, G.-S. (2010) Rockburst characteristics and numerical simulation based on a new energy index: a case study of a tunnel at 2,500 m depth. Bulletin of engineering geology and the environment, Volume 69, No. 3, pp. 381-388.

Kaiser, P. K., and Cai, M. (2012) Design of rock support system under rockburst condition. Journal of Rock Mechanics and Geotechnical Engineering, Volume 4, No. 3, pp. 215-227.

Kias, E., and Ozbay, U. (2013) Modeling Unstable Failure of Coal Pillars in Underground Mining Using the Discrete Element Method. Paper presented at the 47th Rock Mechanics/Geomechanics Symposium. Paper ID: ARMA 13-174.

Manouchehrian, A., and Cai, M. (2016) Simulation of unstable rock failure under unloading conditions. Canadian Geotechnical Journal, Volume 53, No. 1, pp. 22-34.

Milev, A., Spottiswoode, S., Noble, B., Linzer, L., Van Zyl, M., Daehnke, A., and Acheampong, E. (2002) The meaningful use of peak particle velocities at excavation surfaces for the optimisation of the rockburst criteria for tunnels and stopes. SIMRAC Final Project Report GAP, 709.

Wawersik, W. R., & Fairhurst, C. (1970) A study of brittle rock fracture in laboratory compression experiments. International Journal of Rock Mechanics and Mining Sciences & Geomechanics Abstracts. Volume 7, No. 5, pp. 561-575.

Wiles, T. (2002) Loading system stiffness-a parameter to evaluate rockburst potential. Paper presented at the First International Seminar on Deep and High Stress Mining, Australian Centre for Geomechanics, Perth, Australia.

Zhang, C., Feng, X. T., Zhou, H., Qiu, S., and Wu, W. (2012) Case histories of four extremely intense rockbursts in deep tunnels. Rock mechanics and rock engineering, Volume 45, No. 3, pp. 275-288.

Zhang, C., Feng, X. T., Zhou, H., Qiu, S., and Yang, Y. (2014) Rock mass damage induced by rockbursts occurring on tunnel floors: a case study of two tunnels at the Jinping II Hydropower Station. Environmental Earth Sciences, Volume 71, No. 1, pp. 441-450.